Supplementary material: Charge density of the biologically active molecule (2-oxo-1,3-benzoxazol-3(2H)-yl)acetic acid

Ai Wang[a], Jamshid Ashurov[b], Aziz Ibragimov[c], Ruimin Wang[a], Halima Mouhib[d], Nasir Mukhamedov[e] and Ulli Englert*[a]

January 22, 2016

List of Figures

[a] *Institute of Inorganic Chemistry, RWTH Aachen University, Landoltweg 1, Aachen 52074, Germany. Fax: +49 241 8092 288; Tel: +49 241 809 4666 ; E-mail: ullrich.englert@ac.rwth-aachen.de*
[b] *Institute of Bioorganic Chemistry, Academy of Sciences of Uzbekistan, Uzbekistan.*
[c] *Institute of General and Inorganic Chemistry, Academy of Sciences of Uzbekistan,Uzbekistan.*
[d] *Institute of Physical Chemistry, RWTH Aachen University, Germany.*
[e] *Yunusov Institute of the Chemistry of Plant Substances, Academy of Sciences of Uzbekistan, Uzbekistan.*

1 Data collection and completeness

Data collection at standard resolution : a total of 1340 frames in 4 runs with 5 seconds exposure time were measured over a time period of 4 h. A total of 12738 reflections were harvested from the image files. This part of the data set was 99.4 % complete up to a resolution of 0.72 Å and extended to 62 ° in 2θ.
Data collection at high resolution: a total of 2880 frames in 8 runs using 20 seconds exposure time were measured over a time period of 17 h. A total of 59988 reflections were harvested from the image files. The data set was 100.0 % complete up to a resolution of 0.48 Å, and only 24 reflections were missing in the resolution range between 0.48 and 0.46 Å. The maximum resolution in 2θ was 102 °, corresponding to $\sin(\theta_{max})/\lambda = 1.09$.

2 Intensity data merging and multipole model (MM) refinement

The final IAM served as starting point for the multipole model (MM). Data were merged with the help of the program mergehklf5 (Schreurs, 2004). For each reflection, internal $[\Sigma(|(I-<I>)|)/(n\sqrt{(n-1)})]$ and external $[\sqrt{\Sigma(w\cdot\sigma^2)}/(n\cdot\Sigma w)]$ standard uncertainties (su) were calculated and the larger of these values was used as the su of the averaged intensity. In the final multipole refinement, contraction parameters κ and κ' for non-H atoms were freely refined. All C atoms were assigned common contraction parameters, whereas independent κ and κ' were refined for the chemically different O atoms. κ and κ' for H were refined until dipole moments and after then fixed to 1.16 and 0.73, respectively.

3 Bioactivity of (2-oxo-1,3-benzoxazol-3(2H)-yl)acetic acid

The antifungal activity of (2-oxo-1,3-benzoxazol-3(2H)-yl)acetic acid, **(1)** was tested against two common molds with Fluconazole as control. At a concentration of 200 ppm of Fluconazole, growth of Aspergillus niger and Aspergillus flavus was inhibited completely. At the same concentration, **(1)** showed inhibition rates of 85 % towards Aspergillus niger and of 80 % towards Aspergillus flavus with respect to the control experiments (Fig. S18).

4 Theoretical calculations

In order to obtain a more complete overview over the conformational landscape, a two-dimensional potential energy surface (PES), where the carboxylic group and the ring-frame of (2-oxo-1,3-benzoxazol-3(2H)-yl)acetic acid were rotated independently from each other in steps of 10° (θ_1 and θ_2, see Fig.2), was calculated at the B3LYP/6-311++G(d,p) level of theory. The PES was parameterized in a symmetry-adapted two-dimensional Fourier expansion, the Fourier terms and their coefficients are available as supporting information (Table S8 and S9). The range between the global maximum and the global minimum (indicated by a black circle in Fig. 3) is 59.79 kJ/mol, the *ab* initio data points were reproduced from the Fourier expansion with a RMS of 0.38 kJ/mol and a maximum deviation of 2.49 kJ/mol corresponding to less than 4.20 % of the whole range. The complete PES is provided in Fig. 7.

5 Force field calculations

Conformational degrees of freedom were explored with an augmented MM2 force field.(CA Che Program, 2003; Allinger, N. L., 1977) These calculations confirm chemical intuition: an isolated molecule of **(1)** features two relevant torsional degrees of freedom, namely the orientation of the acetyl group with respect to the almost planar benzoxazolone scaffold, and the conformation within the acetyl substituent. The torsion angles C6-N1-C8-C9 and N1-C8-C9-O3 have been systematically varied in steps of 10 °; the remaining molecular geometry was optimized. Fig. S.1 shows the result: the acetyl group adopts a roughly perpendicular orientation to the benzoxazolone; a full scan of the C6-N1-C8-C9 torsion angle involves a barrier of ca. 40 kJ/mol, whereas rotation about N1-C8-C9-O3 is associated with a rather flat energy profile. With respect to the former parameter, the conformation of minimum energy (C6-N1-C8-C9 = 80 °) closely matches the experimentally observed geometry of a molecule of **(1)** in the crystal [91.82(6)°].

6 Rigid bond test

The rigid-bond test (Hirshfeld, 1976) was satisfactory for both refinement models with ΔU_{max} = 0.0009(2) Å^2 for O2-C7 for the IAM and ΔU_{max} = 0.00087(18) Å^2 for N1-C8 for the MM.

7 References

[1] Schreurs, A. M. M. (2004). MERGEHKLF5. Utrecht University, The Netherlands.
[2] CACheProgram, Version 4.9 for Macintosh system, Fujitsu, (2003).
[3] Allinger, N. L. (1977). *J. Am. Chem. Soc.*, **99**, 8127-8134.
[4] Hirshfeld, F. L. (1976). *Acta Cryst.*, A**32**, 239-244.

Tab.S S1: Summary of completeness for the experimental charge density data.

θ	sin(θ)/Λ	Complete	Expected	Measured	Missing
20.82	0.500	1.000	875	875	0
23.01	0.550	1.000	1157	1157	0
25.24	0.600	1.000	1490	1490	0
27.51	0.650	1.000	1917	1917	0
29.84	0.700	1.000	2393	2393	0
32.21	0.750	1.000	2938	2938	0
34.65	0.800	1.000	3553	3553	0
37.17	0.850	1.000	4268	4268	0
39.77	0.900	1.000	5081	5081	0
42.47	0.950	1.000	5954	5954	0
45.29	1.000	1.000	6955	6955	0
48.27	1.050	1.000	8041	8041	0
50.93	1.092	0.997	9068	9043	25

Tab.S S2: R-value statistics as a function of resolution for IAM (in resolution shell)

θ	$\sin(\theta)/\Lambda$	No.	R1	wR2	S	$<I/\sigma W>$	$<I>$	$<\sigma W>$
12.38	0.302	191	0.063	0.166	2.199	12.96	3862.39	267.18
15.68	0.380	190	0.048	0.154	1.854	11.49	1119.90	81.49
18.02	0.435	192	0.038	0.128	1.416	10.47	703.30	55.24
19.90	0.479	192	0.041	0.144	1.530	10.00	813.05	64.71
21.51	0.516	194	0.051	0.140	1.412	9.41	526.24	44.33
22.94	0.548	190	0.055	0.153	1.302	7.49	264.40	24.41
24.22	0.577	191	0.048	0.130	1.121	7.60	241.59	22.85
25.40	0.603	186	0.054	0.156	1.410	8.30	201.17	17.91
26.49	0.628	193	0.049	0.133	1.247	8.58	174.01	15.34
27.52	0.650	198	0.045	0.134	1.246	8.60	154.31	13.57
28.49	0.671	184	0.042	0.114	1.014	8.01	113.69	10.51
29.41	0.691	194	0.042	0.124	1.123	8.21	124.41	11.46
30.28	0.709	193	0.043	0.120	1.007	7.46	105.65	9.97
31.12	0.727	179	0.042	0.112	1.009	8.18	140.39	12.70
31.93	0.744	198	0.042	0.111	0.957	7.74	116.81	10.89
32.71	0.760	194	0.038	0.110	0.931	7.38	101.05	9.73
33.46	0.776	189	0.041	0.111	0.886	6.88	99.69	9.57
34.20	0.791	185	0.049	0.139	1.082	6.89	77.28	7.89
34.91	0.805	176	0.035	0.098	0.739	6.33	71.36	7.47
50.93	1.092	5434	0.058	0.161	0.858	4.00	29.99	4.74

Tab.S S3: Cartesian coordinates of **conf.1** calculated at the B3LYP/6-311++G(d,p) level in the principal axis of inertia.

Atom	a / Å	b / Å	c / Å
C1	-2.0612	0.33719	0.46865
C2	-3.39744	0.04888	0.64018
C3	-3.80823	-1.24516	0.29309
C4	-2.90071	-2.18474	-0.19871
C5	-1.54522	-1.87538	-0.36533
C6	-1.14593	-0.59315	-0.02314
C7	-0.07806	1.36888	0.40779
C8	1.35860	-0.44620	-0.46483
C9	2.01271	-1.31359	0.60539
H1	-4.08748	0.78861	1.02482
H2	-4.84946	-1.51905	0.41194
H3	-3.24862	-3.17865	-0.45345
H4	3.57141	-2.35278	0.84364
H5	-0.84569	-2.61400	-0.73652
H6	2.01971	0.39939	-0.66875
H7	1.26888	-1.02287	-1.38947
N1	0.07955	0.07393	-0.06477
O1	-1.41430	1.52643	0.72843
O2	0.75204	2.22711	0.51898
O3	1.58479	-1.51828	1.70712
O4	3.16975	-1.82969	0.13323

Tab.S S4: Cartesian coordinates of **conf.2** calculated at the B3LYP/6-311++G(d,p) level in the principal axis of inertia.

Atom	a / Å	b / Å	c / Å
C1	3.70879	-1.38943	0.63759
C2	3.35286	-0.04621	0.82136
C3	2.04532	0.28755	0.54388
C4	1.10820	-0.64471	0.09862
C5	1.45249	-1.97511	-0.08270
C6	2.77841	-2.33109	0.19512
C7	0.12543	1.40045	0.25890
C8	-1.36098	-0.44175	-0.48678
C9	-2.13527	-1.21104	0.57993
H1	4.72598	-1.69941	0.84380
H2	4.06224	0.69571	1.16438
H3	0.73509	-2.71212	-0.42228
H4	3.08465	-3.36208	0.06475
H5	-1.97874	0.41233	-0.77733
H6	-1.26103	-1.09213	-1.35777
H7	-2.28084	-1.43359	2.44336
N1	-0.07654	0.07050	-0.08108
O1	-0.66156	2.30429	0.23420
O2	1.45087	1.52739	0.63874
O3	-3.03873	-1.96125	0.31837
O4	-1.72098	-0.93376	1.82945

Tab.S S5: Cartesian coordinates of **conf.3** calculated at the B3LYP/6-311++G(d,p) level in the principal axis of inertia.

Atom	a / Å	b / Å	c / Å
C1	-3.95642	-0.65149	-0.54897
C2	-3.35850	0.60927	-0.66491
C3	-2.00230	0.66588	-0.42890
C4	-1.24376	-0.45393	-0.09091
C5	-1.82942	-1.70549	0.02150
C6	-3.20677	-1.78141	-0.21326
C7	0.09168	1.36897	-0.18405
C8	1.23573	-0.71498	0.54031
C9	2.31898	-0.94814	-0.53062
H1	-5.02024	-0.74994	-0.72654
H2	-3.92311	1.49449	-0.92688
H3	-1.25435	-2.58882	0.26864
H4	-3.69948	-2.74308	-0.13707
H5	1.67950	-0.16398	1.37584
H6	0.91264	-1.68817	0.90003
H7	2.37590	0.96638	-0.79104
N1	0.06587	0.01727	0.06622
O1	1.06090	2.09758	-0.16994
O2	-1.18019	1.77723	-0.48269
O3	2.72746	-2.04887	-0.78313
O4	2.80206	0.14881	-1.12681

Tab.S S6: Cartesian coordinates of **conf.4** calculated at the B3LYP/6-311++G(d,p) level in the principal axis of inertia.

Atom	a / Å	b / Å	c / Å
C1	-3.78575	-1.34079	0.19722
C2	-3.44036	-0.00379	0.43494
C3	-2.10615	0.31619	0.30901
C4	-1.13530	-0.62344	-0.03125
C5	-1.46870	-1.94774	-0.26803
C6	-2.82165	-2.28917	-0.14918
C7	-0.16398	1.42457	0.21756
C8	1.34402	-0.39398	-0.58441
C9	2.13362	-1.35070	0.31908
H1	-4.82289	-1.64102	0.28274
H2	-4.17694	0.74367	0.69925
H3	-0.72418	-2.68954	-0.52954
H4	-3.12239	-3.31448	-0.32699
H5	1.18949	-0.89436	-1.54213
H6	1.97007	0.48560	-0.75590
H7	1.15843	-0.65704	1.80912
N1	0.08293	0.07453	-0.04051
O1	0.61947	2.32995	0.23380
O2	-1.51481	1.55246	0.47509
O3	2.96883	-2.08508	-0.12570
O4	1.86483	-1.29646	1.63845

Tab.S S7: Cartesian coordinates of **conf.5** calculated at the B3LYP/6-311++G(d,p) level in the principal axis of inertia.

Atom	a / Å	b / Å	c / Å
C1	3.80547	-1.26297	0.24098
C2	3.40778	0.03543	0.58587
C3	2.07050	0.32942	0.43347
C4	1.14225	-0.59923	-0.03560
C5	1.52803	-1.88661	-0.37320
C6	2.88443	-2.20124	-0.22817
C7	0.09586	1.37625	0.39496
C8	-1.36523	-0.41785	-0.46748
C9	-2.01090	-1.35696	0.56148
H1	4.84683	-1.54214	0.34501
H2	4.10772	0.77397	0.95444
H3	0.81694	-2.62723	-0.71674
H4	3.22208	-3.19976	-0.47840
H5	-2.01190	0.45230	-0.61518
H6	-1.27817	-0.94158	-1.42680
H7	-3.53851	-1.41988	-0.62567
N1	-0.08039	0.07620	-0.05859
O1	-0.72774	2.24203	0.50254
O2	1.43471	1.52547	0.69612
O3	-1.50177	-1.69403	1.58688
O4	-3.23926	-1.81262	0.20448

Tab.S S8: Fourier coefficient of the PES shown in Fig. 7 of the manuscript. All ab initio data points are reproduced within 4.2 %. The potential energy is obtained from $V(\theta_1, \theta_2) = \sum_{i=1}^{169} V_i f_i$

i	V_i/ Hartree	f_i	i	V_i/ Hartree	f_i
1	-703.047887	1	46	0.000012	$\cos(6*\theta_2) * \cos(1*\theta_1)$
2	-0.000536	$\cos(1*\theta_2)$	47	-0.000001	$\sin(6*\theta_2) * \sin(1*\theta_1)$
3	-0.000004	$\sin(1*\theta_2)$	48	-0.000002	$\cos(6*\theta_2) * \sin(1*\theta_1)$
4	-0.001907	$\cos(1*\theta_1)$	49	0.000001	$\sin(6*\theta_2) * \cos(1*\theta_1)$
5	0.000632	$\sin(1*\theta_1)$	50	-0.000131	$\cos(1*\theta_2) * \cos(2*\theta_1)$
6	-0.000450	$\cos(2*\theta_2)$	51	0.000462	$\sin(1*\theta_2) * \sin(2*\theta_1)$
7	-0.000046	$\sin(2*\theta_2)$	52	0.000088	$\cos(1*\theta_2) * \sin(2*\theta_1)$
8	0.005086	$\cos(2*\theta_1)$	53	0.000190	$\sin(1*\theta_2) * \cos(2*\theta_1)$
9	-0.001594	$\sin(2*\theta_1)$	54	0.002771	$\cos(2*\theta_2) * \cos(2*\theta_1)$
10	-0.000380	$\cos(3*\theta_2)$	55	-0.003698	$\sin(2*\theta_2) * \sin(2*\theta_1)$
11	0.000002	$\sin(3*\theta_2)$	56	-0.000779	$\cos(2*\theta_2) * \sin(2*\theta_1)$
12	0.000714	$\cos(3*\theta_1)$	57	-0.001114	$\sin(2*\theta_2) * \cos(2*\theta_1)$
13	-0.000061	$\sin(3*\theta_2)$	58	-0.000315	$\cos(3*\theta_2) * \cos(2*\theta_1)$
14	-0.000013	$\cos(4*\theta_2)$	59	0.000395	$\sin(3*\theta_2) * \sin(2*\theta_1)$
15	0.000003	$\sin(4*\theta_2)$	60	0.000106	$\cos(3*\theta_2) * \sin(2*\theta_1)$
16	0.000231	$\cos(4*\theta_1)$	61	0.000131	$\sin(3*\theta_2) * \cos(2*\theta_1)$
17	-0.000238	$\sin(4*\theta_1)$	62	0.000179	$\cos(4*\theta_2) * \cos(2*\theta_1)$
18	0.000015	$\cos(5*\theta_2)$	63	-0.000082	$\sin(4*\theta_2) * \sin(2*\theta_1)$
19	0.000000	$\sin(5*\theta_2)$	64	-0.000048	$\cos(4*\theta_2) * \sin(2*\theta_1)$
20	-0.000069	$\cos(5*\theta_1)$	65	-0.000010	$\sin(4*\theta_2) * \cos(2*\theta_1)$
21	0.000043	$\sin(5*\theta_1)$	66	-0.000038	$\cos(5*\theta_2) * \cos(2*\theta_1)$
22	0.000032	$\cos(6*\theta_2)$	67	0.000051	$\sin(5*\theta_2) * \sin(2*\theta_1)$
23	0.000000	$\sin(6*\theta_2)$	68	0.000012	$\cos(5*\theta_2) * \sin(2*\theta_1)$
24	-0.000037	$\cos(6*\theta_1)$	69	0.000018	$\sin(5*\theta_2) * \cos(2*\theta_1)$
25	0.000050	$\sin(6*\theta_1)$	70	0.000003	$\cos(6*\theta_2) * \cos(2*\theta_1)$
26	-0.001259	$\cos(1*\theta_2) * \cos(1*\theta_1)$	71	-0.000014	$\sin(6*\theta_2) * \sin(2*\theta_1)$
27	0.000894	$\sin(1*\theta_2) * \sin(1*\theta_1)$	72	-0.000002	$\cos(6*\theta_2) * \sin(2*\theta_1)$
28	0.000188	$\cos(1*\theta_2) * \sin(1*\theta_1)$	73	-0.000005	$\sin(6*\theta_2) * \cos(2*\theta_1)$
29	0.000106	$\sin(1*\theta_2) * \cos(1*\theta_1)$	74	-0.000325	$\cos(1*\theta_2) * \cos(3*\theta_1)$
30	-0.000371	$\cos(2*\theta_2) * \cos(1*\theta_1)$	75	0.000416	$\sin(1*\theta_2) * \sin(3*\theta_1)$
31	0.000991	$\sin(2*\theta_2) * \sin(1*\theta_1)$	76	0.000219	$\cos(1*\theta_2) * \sin(3*\theta_1)$
32	0.000010	$\cos(2*\theta_2) * \sin(1*\theta_1)$	77	0.000227	$\sin(1*\theta_2) * \cos(3*\theta_1)$
33	0.000122	$\sin(2*\theta_2) * \cos(1*\theta_1)$	78	-0.000963	$\cos(2*\theta_2) * \cos(3*\theta_1)$
34	0.000049	$\cos(3*\theta_2) * \cos(1*\theta_1)$	79	0.000928	$\sin(2*\theta_2) * \sin(3*\theta_1)$
35	-0.000054	$\sin(3*\theta_2) * \sin(1*\theta_1)$	80	0.000807	$\cos(2*\theta_2) * \sin(3*\theta_1)$
36	-0.000035	$\cos(3*\theta_2) * \sin(1*\theta_1)$	81	0.000819	$\sin(2*\theta_2) * \cos(3*\theta_1)$
37	-0.000034	$\sin(3*\theta_2) * \cos(1*\theta_1)$	82	0.000105	$\cos(3*\theta_2) * \cos(3*\theta_1)$
38	0.000018	$\cos(4*\theta_2) * \cos(1*\theta_1)$	83	-0.000130	$\sin(3*\theta_2) * \sin(3*\theta_1)$
39	-0.000115	$\sin(4*\theta_2) * \sin(1*\theta_1)$	84	-0.000102	$\cos(3*\theta_2) * \sin(3*\theta_1)$
40	0.000006	$\cos(4*\theta_2) * \sin(1*\theta_1)$	85	-0.000119	$\sin(3*\theta_2) * \cos(3*\theta_1)$
41	-0.000003	$\sin(4*\theta_2) * \cos(1*\theta_1)$	86	0.000017	$\cos(4*\theta_2) * \cos(3*\theta_1)$
42	0.000012	$\cos(5*\theta_2) * \cos(1*\theta_1)$	87	0.000014	$\sin(4*\theta_2) * \sin(3*\theta_1)$
43	-0.000020	$\sin(5*\theta_2) * \sin(1*\theta_1)$	88	0.000005	$\cos(4*\theta_2) * \sin(3*\theta_1)$
44	-0.000002	$\cos(5*\theta_2) * \sin(1*\theta_1)$	89	0.000026	$\sin(4*\theta_2) * \cos(3*\theta_1)$
45	-0.000003	$\sin(5*\theta_2) * \cos(1*\theta_1)$	90	0.000010	$\cos(5*\theta_2) * \cos(3*\theta_1)$

Tab.S S9: Fourier coefficient of the PES shown in Fig. 7 of the manuscript. All ab initio data points are reproduced within 4.2 %. The potential energy is obtained from $V(\theta_1, \theta_2) = \sum_{i=1}^{169} V_i f_i$

i	V_i/ Hartree	f_i	i	V_i/ Hartree	f_i
91	-0.000003	sin(5*θ_2) * sin(3*θ_1)	136	0.000055	cos(4*θ_2) * sin(5*θ_1)
92	-0.000004	cos(5*θ_2) * sin(3*θ_1)	137	0.000057	sin(4*θ_2) * cos(5*θ_1)
93	-0.000004	sin(5*θ_2) * cos(3*θ_1)	138	0.000017	cos(5*θ_2) * cos(5*θ_1)
94	0.000002	cos(6*θ_2) * cos(3*θ_1)	139	-0.000018	sin(5*θ_2) * sin(5*θ_1)
95	-0.000007	sin(6*θ_2) * sin(3*θ_1)	140	-0.000001	cos(5*θ_2) * sin(5*θ_1)
96	0.000003	cos(6*θ_2) * sin(3*θ_1)	141	-0.000002	sin(5*θ_2) * cos(5*θ_1)
97	0.000000	sin(6*θ_2) * cos(3*θ_1)	142	-0.000010	cos(6*θ_2) * cos(5*θ_1)
98	0.000151	cos(1*θ_2) * cos(4*θ_1)	143	0.000011	sin(6*θ_2) * sin(5*θ_1)
99	-0.000036	sin(1*θ_2) * sin(4*θ_1)	144	0.000009	cos(6*θ_2) * sin(5*θ_1)
100	-0.000096	cos(1*θ_2) * sin(4*θ_1)	145	0.000011	sin(6*θ_2) * cos(5*θ_1)
101	0.000017	sin(1*θ_2) * cos(4*θ_1)	146	0.000030	cos(1*θ_2) * cos(6*θ_1)
102	0.000860	cos(2*θ_2) * cos(4*θ_1)	147	-0.000043	sin(1*θ_2) * sin(6*θ_1)
103	-0.000984	sin(2*θ_2) * sin(4*θ_1)	148	-0.000043	cos(1*θ_2) * sin(6*θ_1)
104	-0.000647	cos(2*θ_2) * sin(4*θ_1)	149	-0.000061	sin(1*θ_2) * cos(6*θ_1)
105	-0.000755	sin(2*θ_2) * cos(4*θ_1)	150	0.000086	cos(2*θ_2) * cos(6*θ_1)
106	-0.000211	cos(3*θ_2) * cos(4*θ_1)	151	-0.000067	sin(2*θ_2) * sin(6*θ_1)
107	0.000206	sin(3*θ_2) * sin(4*θ_1)	152	-0.000147	cos(2*θ_2) * sin(6*θ_1)
108	0.000178	cos(3*θ_2) * sin(4*θ_1)	153	-0.000107	sin(2*θ_2) * cos(6*θ_1)
109	0.000169	sin(3*θ_2) * cos(4*θ_1)	154	-0.000010	cos(3*θ_2) * cos(6*θ_1)
110	0.000167	cos(4*θ_2) * cos(4*θ_1)	155	0.000013	sin(3*θ_2) * sin(6*θ_1)
111	-0.000150	sin(4*θ_2) * sin(4*θ_1)	156	0.000029	cos(3*θ_2) * sin(6*θ_1)
112	-0.000116	cos(4*θ_2) * sin(4*θ_1)	157	0.000035	sin(3*θ_2) * cos(6*θ_1)
113	-0.000095	sin(4*θ_2) * cos(4*θ_1)	158	0.000087	cos(4*θ_2) * cos(6*θ_1)
114	-0.000026	cos(5*θ_2) * cos(4*θ_1)	159	-0.000095	sin(4*θ_2) * sin(6*θ_1)
115	0.000030	sin(5*θ_2) * sin(4*θ_1)	160	-0.000114	cos(4*θ_2) * sin(6*θ_1)
116	0.000014	cos(5*θ_2) * sin(4*θ_1)	161	-0.000122	sin(4*θ_2) * cos(6*θ_1)
117	0.000017	sin(5*θ_2) * cos(4*θ_1)	162	-0.000035	cos(5*θ_2) * cos(6*θ_1)
118	0.000022	cos(6*θ_2) * cos(4*θ_1)	163	0.000033	sin(5*θ_2) * sin(6*θ_1)
119	-0.000026	sin(6*θ_2) * sin(4*θ_1)	164	0.000048	cos(5*θ_2) * sin(6*θ_1)
120	-0.000016	cos(6*θ_2) * sin(4*θ_1)	165	0.000043	sin(5*θ_2) * cos(6*θ_1)
121	-0.000020	sin(6*θ_2) * cos(4*θ_1)	166	0.000021	cos(6*θ_2) * cos(6*θ_1)
122	-0.000053	cos(1*θ_2) * cos(5*θ_1)	167	-0.000021	sin(6*θ_2) * sin(6*θ_1)
123	0.000026	sin(1*θ_2) * sin(5*θ_1)	168	-0.000036	cos(6*θ_2) * sin(6*θ_1)
124	0.000058	cos(1*θ_2) * sin(5*θ_1)	169	-0.000033	sin(6*θ_2) * cos(6*θ_1)
125	0.000053	sin(1*θ_2) * cos(5*θ_1)			
126	-0.000229	cos(2*θ_2) * cos(5*θ_1)			
127	0.000253	sin(2*θ_2) * sin(5*θ_1)			
128	0.000225	cos(2*θ_2) * sin(5*θ_1)			
129	0.000225	sin(2*θ_2) * cos(5*θ_1)			
130	0.000064	cos(3*θ_2) * cos(5*θ_1)			
131	-0.000062	sin(3*θ_2) * sin(5*θ_1)			
132	-0.000072	cos(3*θ_2) * sin(5*θ_1)			
133	-0.000073	sin(3*θ_2) * cos(5*θ_1)			
134	-0.000101	cos(4*θ_2) * cos(5*θ_1)			
135	0.000093	sin(4*θ_2) * sin(5*θ_1)			

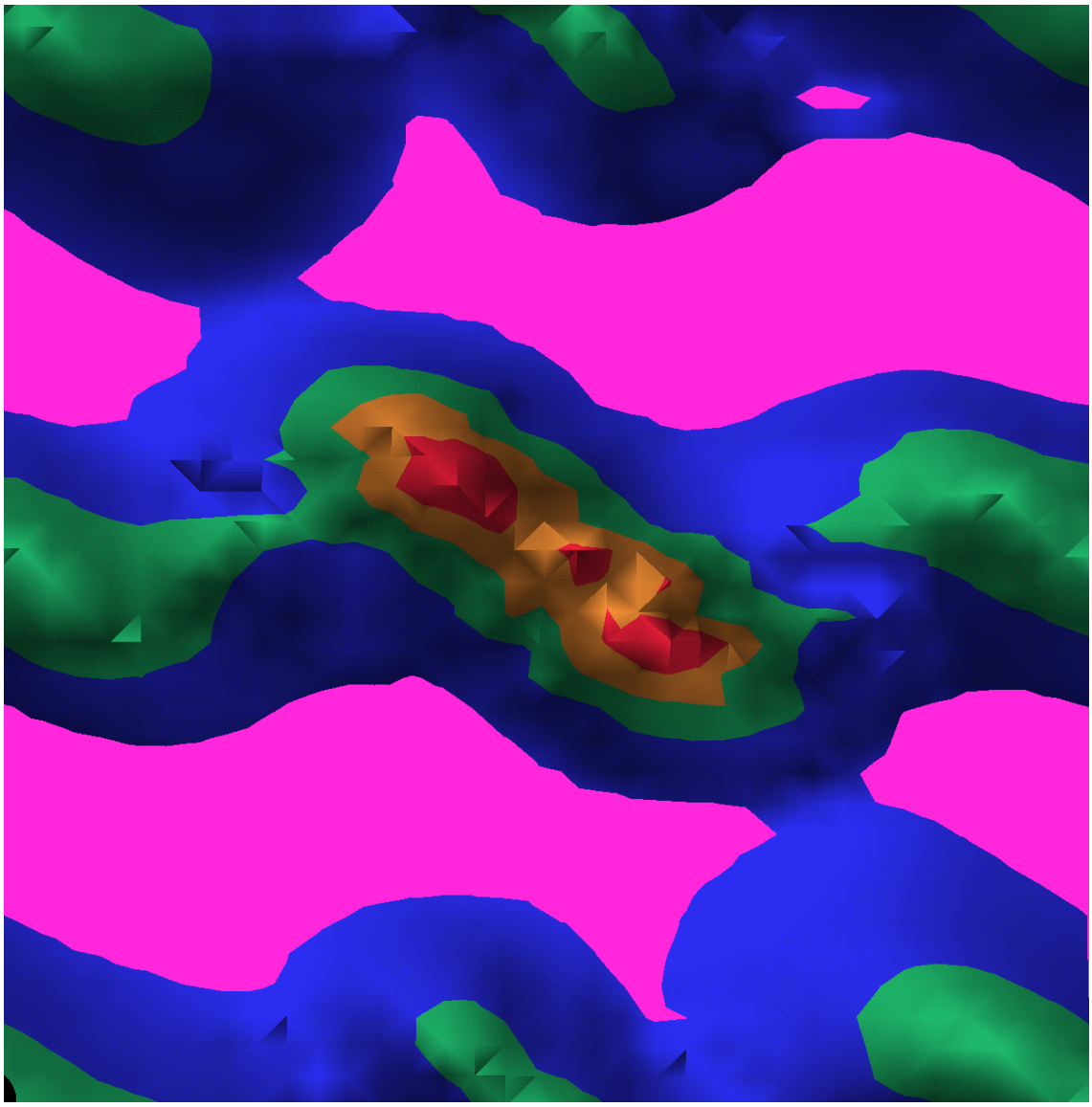

Fig.S 1: Potential energy surface for **(1)** based on force field calculations. Energy range from -49.9 to +14.20 kJ / mol; colour code magenta (lowest energy), blue, greeen, orange, red (highest energy).

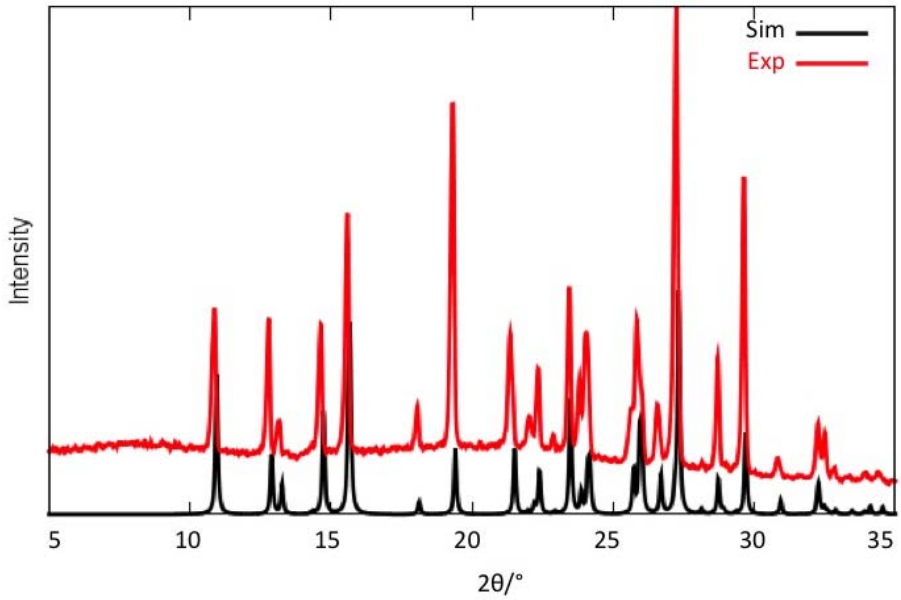

Fig.S 2: Experimental (red) and simulated (black) powder pattern for **(1)**.

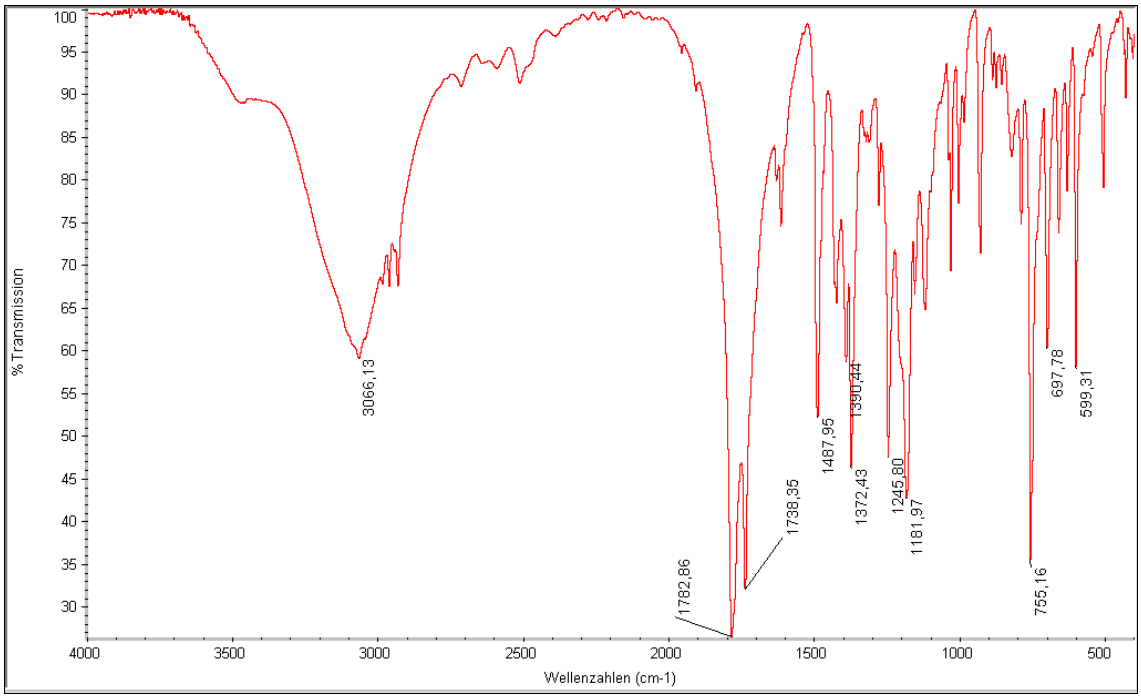

Fig.S 3: IR spectrum for **(1)**.

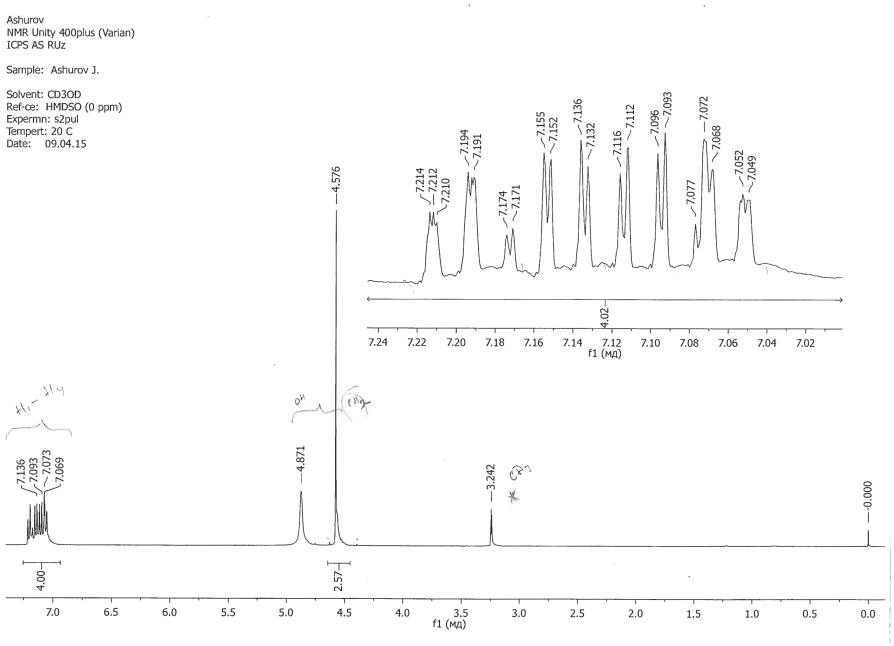

Fig.S 4: NMR spectrum for **(1)**.

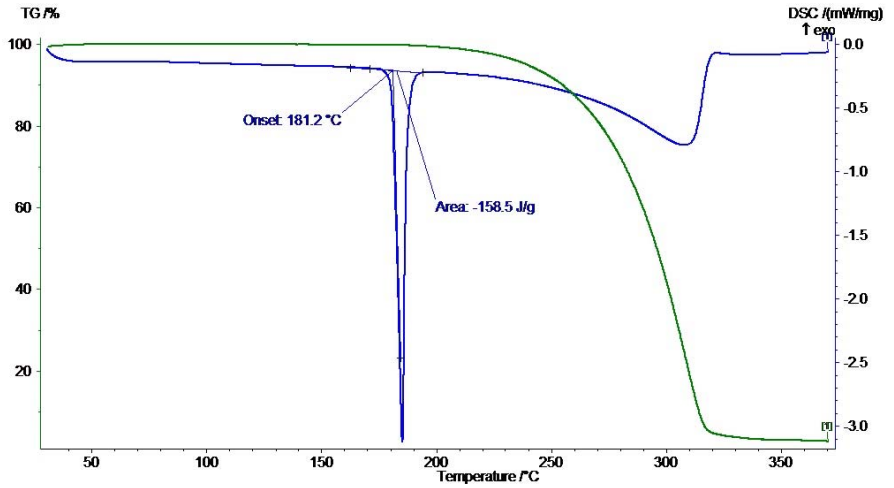

Fig.S 5: Thermal analysis for **(1)**.

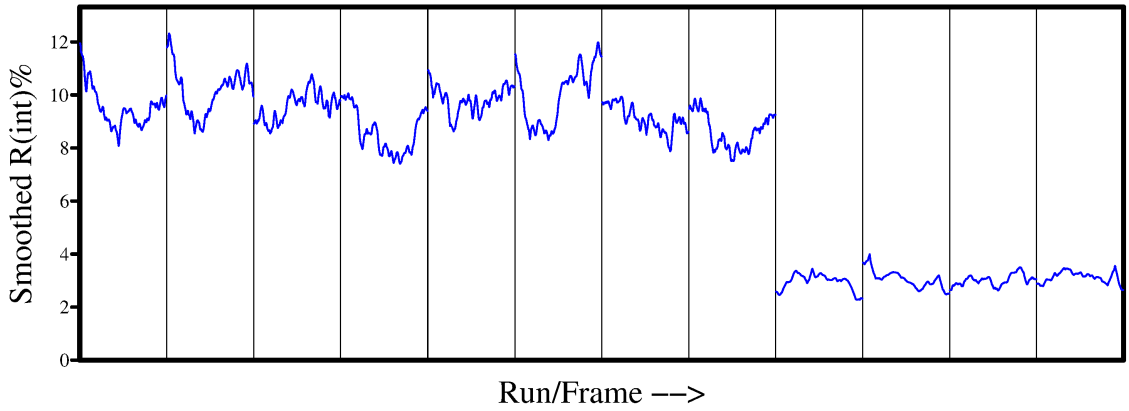

Fig.S 6: Smoothed R(int) % vs run number in the intensity data for **(1)**.

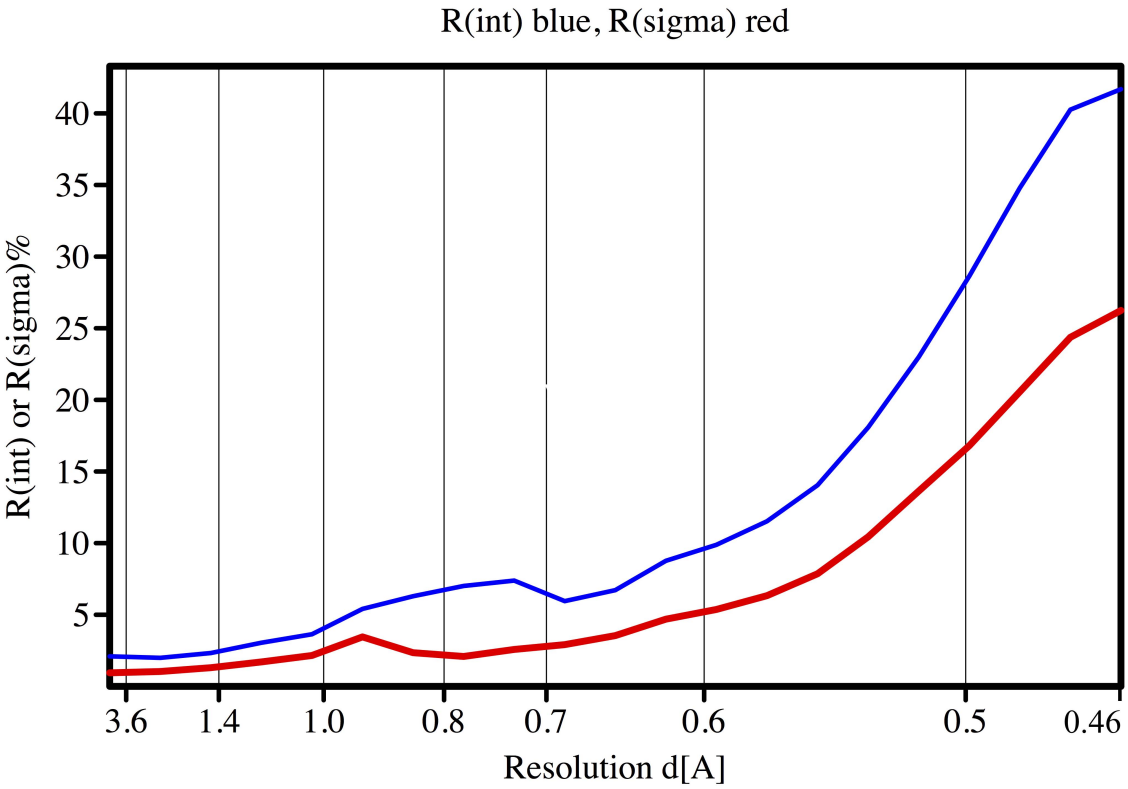

Fig.S 7: R(int) and R(sigma) as a function of the resolution for **(1)**.

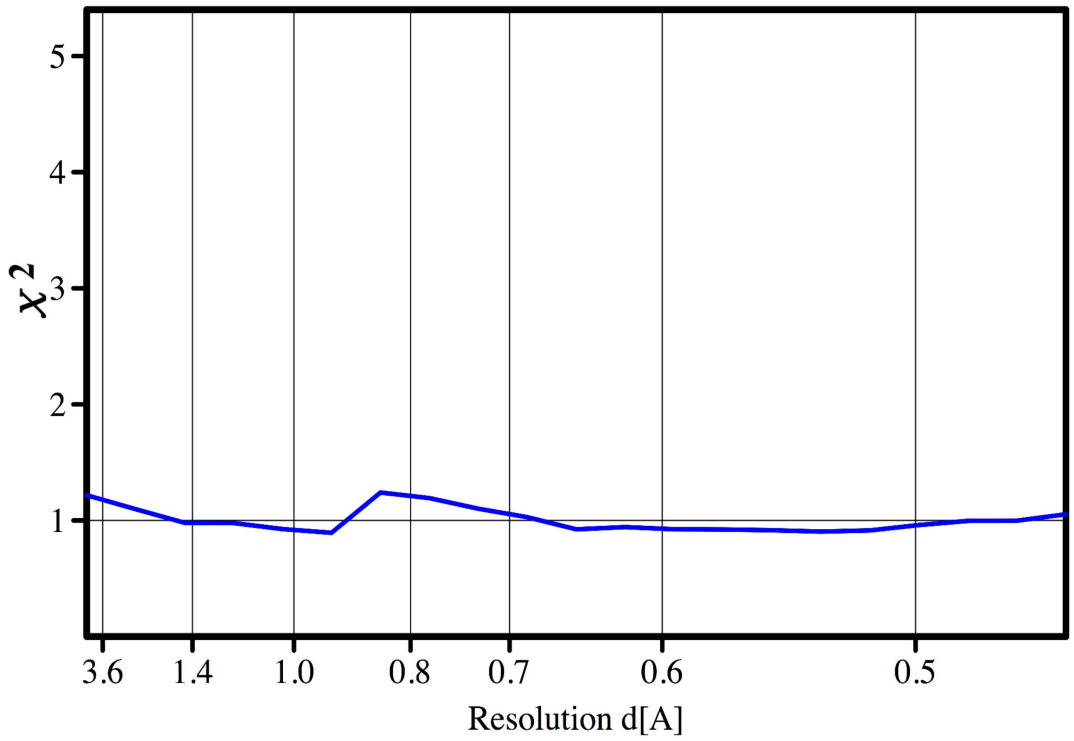

Fig.S 8: χ^2 vs resolution in the intensity data for **(1)**.

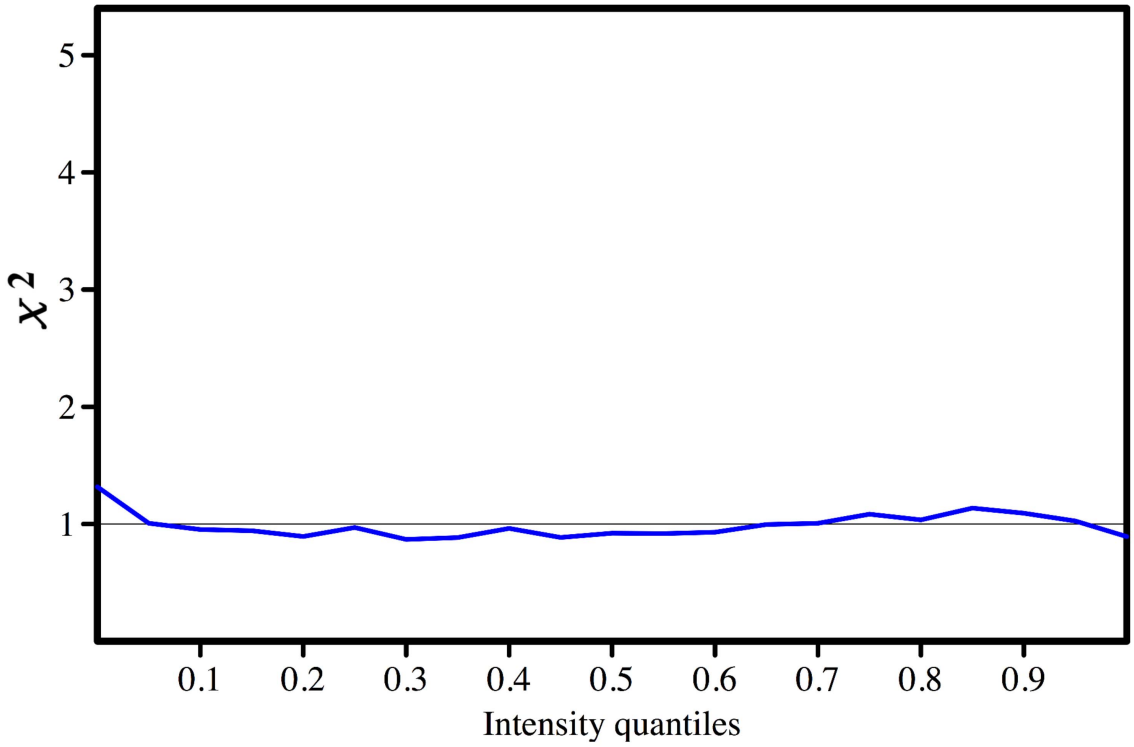

Fig.S 9: χ^2 vs intensity quantiles in the intensity data for **(1)**.

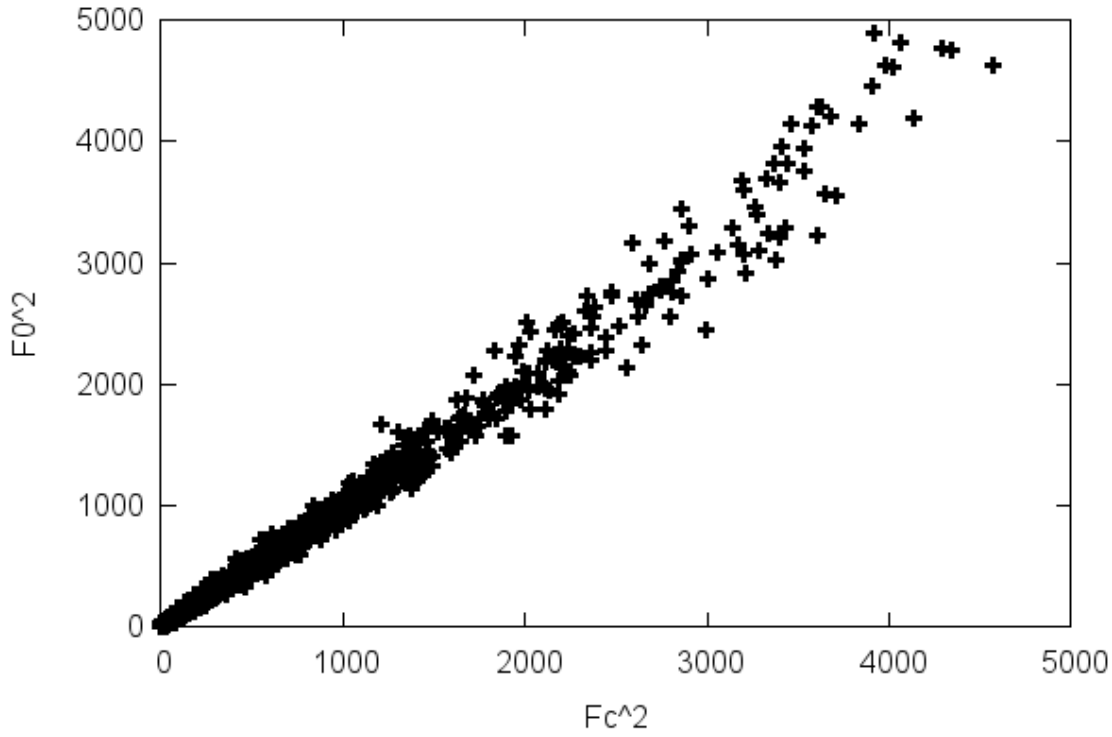

Fig.S 10: Scatterplot F^2_{obs} vs F^2_{calc} for X-ray refinement result (IAM) for **(1)**.

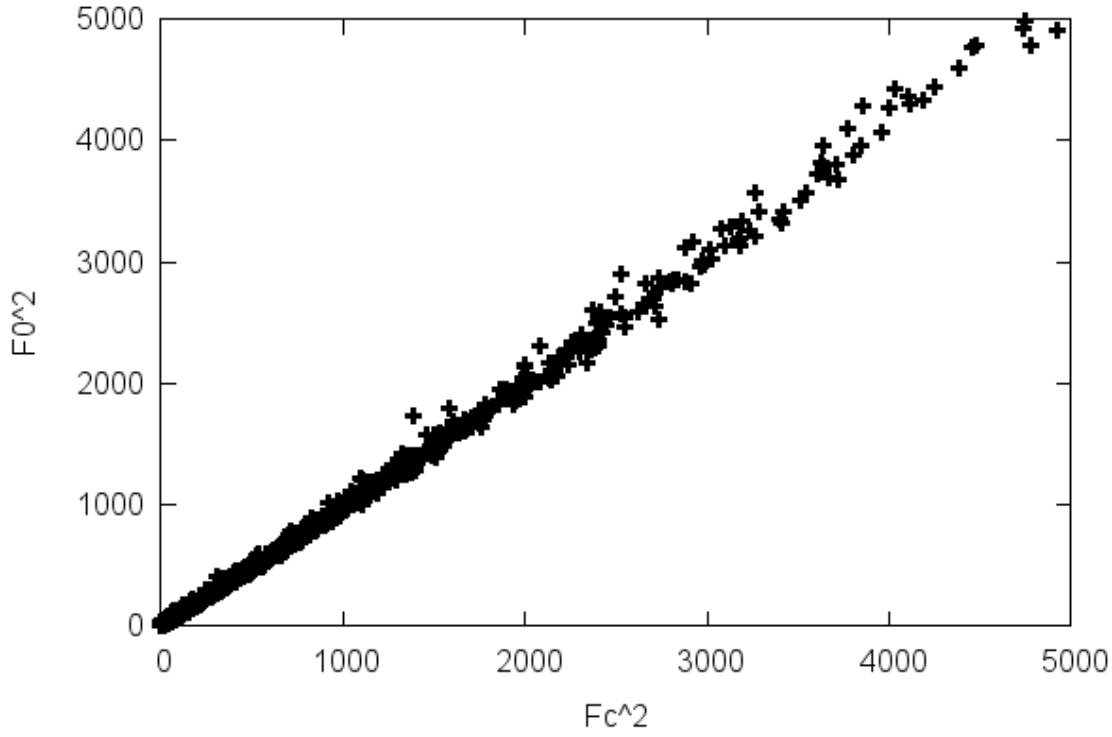

Fig.S 11: Scatterplot F^2_{obs} vs F^2_{calc} for charge density refinement result (MM) for **(1)**.

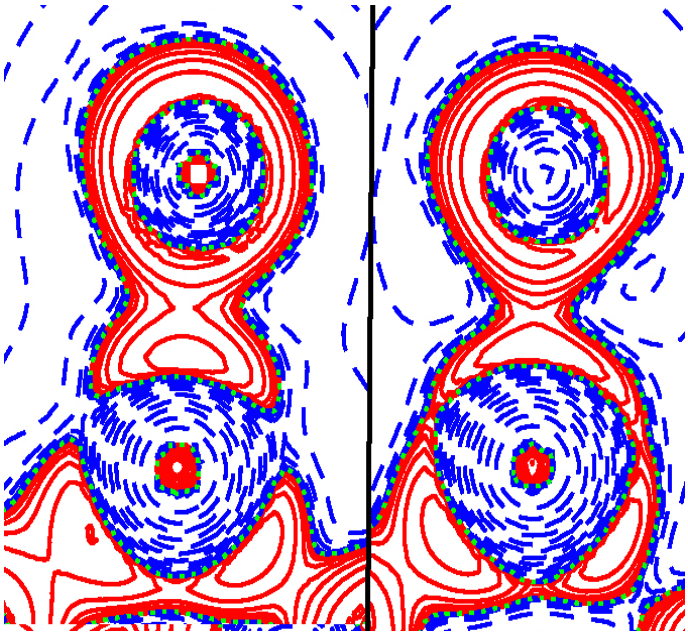

Fig.S 12: Laplacian in the region of the carbonyl group C7=O2.

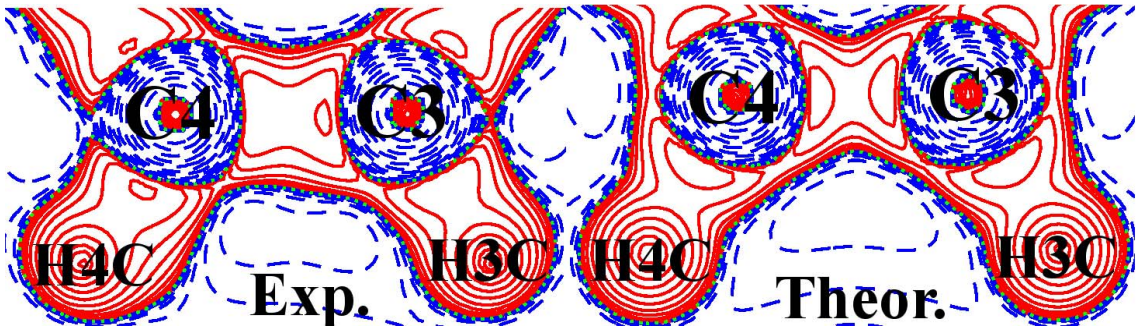

Fig.S 13: Laplacian of sections: C4-H4C / C3-H3C.

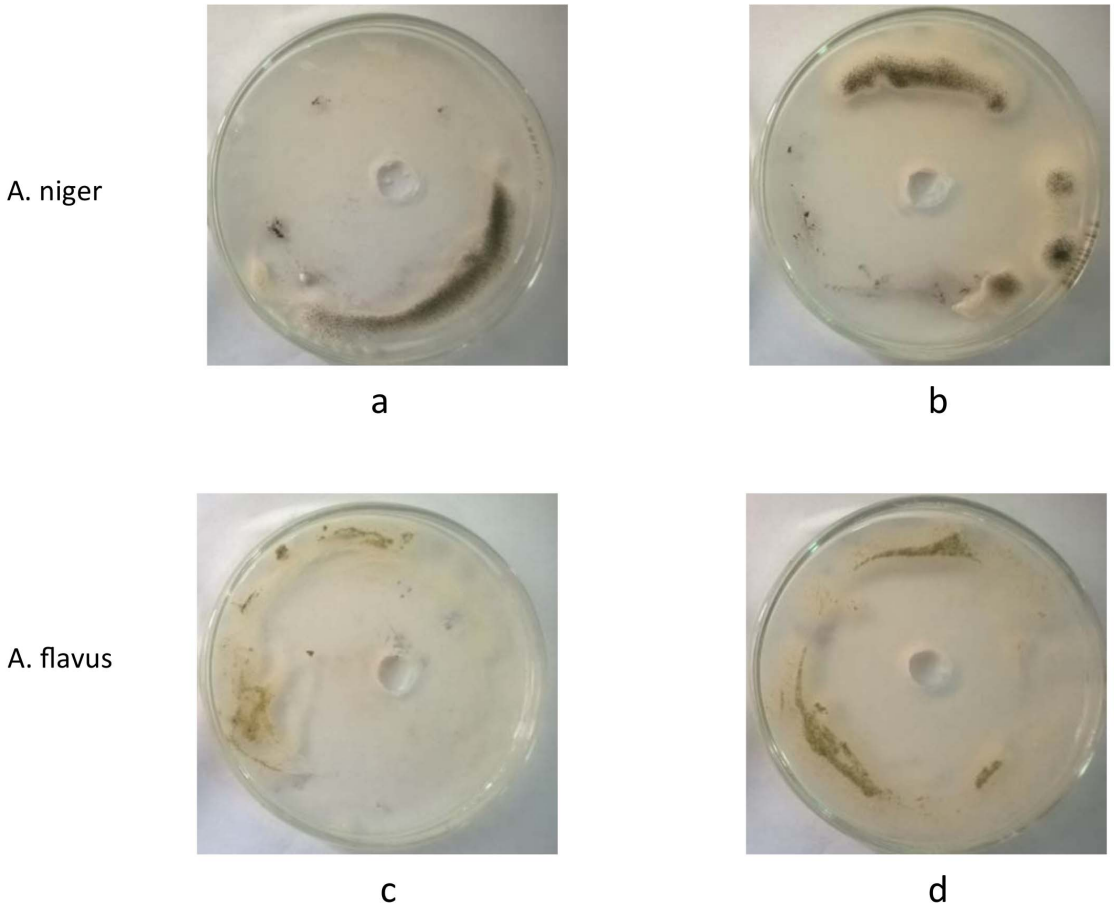

Fig.S 14: The outcome of four experiments with respect to antifungal activity of **(1)**. **(1)** showed inhibition rates of 85 % towards Aspergillus niger (a,b) and of 80 % for flavus (c,d) with respect to the control experiments.